Evaluation of the ZrO_2/Al_2O_3 system as catalysts in the catalytic transfer hydrogenation of furfural to obtain furfuryl alcohol

C. García-Sancho (Investigation) (Data curation)<ce:contributor-role>Writing - Review and Editing), C.P. Jiménez-Gómez (Investigation) (Data curation)<ce:contributor-role>Writing - Original Draft) (Visualization), N. Viar-Antuñano (Investigation) (Data curation), J.A. Cecilia (Conceptualization) (Methodology) (Data curation)<ce:contributor-role>Writing - Original Draft)<ce:contributor-role>Writing - Review and Editing) (Visualization) (Supervision), R. Moreno-Tost (Data curation)<ce:contributor-role>Writing - Review and Editing), J.M. Mérida-Robles (Conceptualization)<ce:contributor-role>Writing - Original Draft)<ce:contributor-role>Writing - Review and Editing) (Supervision), J. Requies (Data curation)<ce:contributor-role>Writing - Review and Editing) (Supervision), P. Maireles-Torres (Methodology) (Resources) (Investigation)<ce:contributor-role>Writing - Original Draft)<ce:contributor-role>Writing - Review and Editing) (Supervision) (Project administration) (Funding acquisition)

PII: S0926-860X(20)30498-1

DOI: https://doi.org/10.1016/j.apcata.2020.117905

Reference: APCATA 117905

To appear in: *Applied Catalysis A, General*

Received Date: 19 May 2020

Revised Date: 21 October 2020

Accepted Date: 26 October 2020

Please cite this article as: García-Sancho C, Jiménez-Gómez CP, Viar-Antuñano N, Cecilia JA, Moreno-Tost R, Mérida-Robles JM, Requies J, Maireles-Torres P, Evaluation of the ZrO_2/Al_2O_3 system as catalysts in the catalytic transfer hydrogenation of furfural to obtain furfuryl alcohol, *Applied Catalysis A, General* (2020), doi: https://doi.org/10.1016/j.apcata.2020.117905

Evaluation of the ZrO_2/Al_2O_3 system as catalysts in the catalytic transfer hydrogenation of furfural to obtain furfuryl alcohol

C. García-Sancho[a], C.P. Jiménez-Gómez[a], N. Viar-Antuñano[b], J.A. Cecilia[a,*], R. Moreno-Tost[a], J.M. Mérida-Robles[a,*], J. Requies[b], P. Maireles-Torres[a]

[a] Universidad de Málaga, Departamento de Química Inorgánica, Cristalografía y Mineralogía (Unidad Asociada al ICP-CSIC), Facultad de Ciencias, Campus de Teatinos, 29071 Málaga, Spain.

[b] Dept. of Chemical and Environmental Engineering, School of Engineering, University of the Basque Country (UPV/EHU), c/Alda. Urquijo s/n, 48013 Bilbao, Spain

*Corresponding author: jacecilia@uma.es, jmerida@uma.es

Graphical Abstract

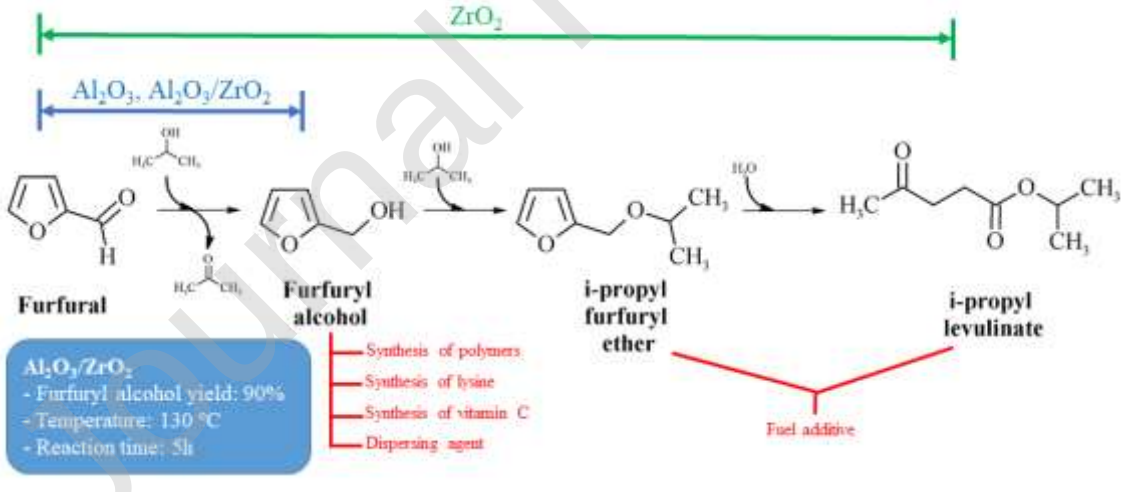

Highlights

- ZrO_2, Al_2O_3 and ZrO_2/Al_2O_3 have been synthesized by coprecipitation method obtaining catalysts with small crystal size, high surface area and high amount of acid sites.

- All catalysts were active in the hydrogen catalytic transfer reaction of furfural to furfuryl alcohol, being ZrO_2/Al_2O_3 the most active catalysts.
- The catalytic activity is directly related to the textural properties and the amount of available acid sites.
- ZrO_2 catalyst also promoted the etherification of furfural obtainin i-propylfurfuryl ether and i-propyl levulinate.

Abstract

ZrO_2, Al_2O_3 and ZrO_2/Al_2O_3, with different Zr/Al molar ratio, have been synthesized by coprecipitation and subsequent calcination. The resulting catalysts were characterized by X-ray diffraction, transmission electronic microscopy, N_2 adsorption-desorption at -196 ºC, CO_2-thermoprogrammed desorption, NH_3-thermoprogrammed desorption and X-ray photoelectronic microscopy. Then, the catalysts were evaluated in the Meenwein-Ponndorf-Verley reduction of furfural (FUR) using 2-propanol as sacrificing alcohol. The catalyst with a Zr/Al molar ratio of 1, Zr_5Al_5, reached the highest conversion value in shorter reaction times, attaining a FUR conversion of 95% with a yield of furfuryl alcohol (FOL) above 90% after 5 h of reaction at 130 °C, due to its greater amount of acid sites as well as higher specific surface area and pore volume.

Keywords: ZrO_2/Al_2O_3 catalysts; heterogeneous catalysts; furfural; furfuryl alcohol; catalytic transfer hydrogenation

1. Introduction.

Industrial development and the increase in world population has caused an increase in energy demands. This has resulted in the depletion of fossil fuels and the extraction of lower quality and more polluting fossil fuels. This fact together with the most restrictive environmental regulations has led to the search for energy sources and chemical products that are highly available throughout the planet and, in turn, are more environmentally friendly.

Nowadays, biomass has emerged as sustainable alternative to replace traditional fossil resources, since it is the only that can provide fuels and chemicals [1]. In spite of biomass is widely distributed worldwide, this must be carefully selected because it could interfere with the food chain, causing an increase in the cost of food, responsible of speculation and social imbalances.

Considering these premises, lignocellulose has become a sustainable source of biomass due to being considered as a waste, whose price is negligible in most of cases. Lignocellulosic biomass is composed by lignin (15-25%), cellulose (40-50%) and hemicellulose (20-35%). Concerning hemicellulose, mainly formed by xylans, it may be isolated of the remaining fractions and subsequently hydrolyzed in their C5 and C6 monomers, mainly xylose [2]. Next, xylose can be dehydrated through acid catalysis to produce furfural (FUR) [2].

Currently, after bioethanol, FUR is the main product obtained from the sugar platform of a biorefinery. Its high interest is ascribed to its physicochemical properties, because it can be used for the synthesis of resins and adhesives, as well as fungicides or nematocides [3]. These applications are associated to its high reactivity conferred by both a furan ring and an aldehyde group [3]. In this sense, FUR can undergo hydrogenation, decarbonylation, oxidation, dehydration, condensation, esterification or ring opening reactions to obtain a wide range of valuable products, some of them now synthesized in the petrochemical industry. [4].

From a yearly furfural production around 280000 Tm in the last decade [3,4], around 62% is estimated to be transformed into furfuryl alcohol (FOL) [4]. The great interest of this compound is due to its industrial relevance for the manufacture of foundry resins [5], used in the synthesis of cross-linked polymers with itself or furfural, formaldehyde,

phenolic compounds or urea, obtaining resins with excellent mechanical and thermochemical properties, as well as high resistance to corrosion and solvent action [5]. Taking into account the important FOL production, the scientific community is searching efficient catalysts to develop competitive and sustainable processes. Quaker Oats Company carried out the first study in 1932, by using copper supported on $Na_2O.xSiO_2$ as catalyst, reaching a FOL yield of 99 % at 170 ºC [6]. Industrially, FOL is produced through a hydrogenation process, using a copper chromite catalyst. However, this catalyst is prone to deactivation and Cr species are harmful for health and environment [6], in such a way that the design of alternative active and selective Cr-free catalysts is required. Most of studies have been performed by using transition metal-based catalysts, mainly Cu, Ni, Pd [7], through gas- and liquid-phase reactions. In the case of gas-phase hydrogenation, progressive deactivation of catalysts, as a consequence of the strong interaction of FUR with active sites, is an important drawback. In addition, both the hydrogenating character of metal sites and the amount of acid and basic sites have to be modulated to avoid the formation of a large spectrum of products by undesired catalytic processes [7–11]. In liquid-phase, the catalyst deactivation is less pronounced, although more severe pressure and temperature are required in most of cases [4,6].

On the other hand, catalytic transfer hydrogenation (CTH), using an alcohol as hydrogen donor, has emerged as a potential alternative to replace H_2 for the reduction of aldehydes and ketones into alcohols. The main advantages of CTH reactions are associated to the use of metal-free catalysts and milder experimental conditions [12].

Although CTH processes have been already reported for biomass hydrogenation, the earlier studies were carried out independently by Meerwein, Ponndorf, and Verley (MPV), in 1925-1926 [13–15]. This reaction requires the participation of Lewis acid sites to promote hydrogen migration from primary and, mainly, secondary alcohols to the carbonyl group of aldehyde, or ketone, through a six-membered intermediate [12–16]. Initially, homogeneous Lewis catalysts formed through complexes or alkoxides were used for CTH [17–19]. In recent years, much attention is being paid to the development of heterogeneous catalysts, due to the easy separation of catalysts from the reaction medium and the ability to be reused. In this sense, several metal oxides (M_xO_y), such as ZrO_2 [20–23], Al_2O_3 [22,24,25], Fe_2O_3 [26], Fe_3O_4 [27,28], MgO [22,29,30] or

zeolites modified with tetravalent species, such as Zr^{4+} [31,32], Sn^{4+} [33–36] or Hf^{4+}, [37,38], have been reported as efficient catalysts in the MPV reaction of FUR. It has been pointed out that the presence of well-dispersed Zr^{4+} species on porous silica also allows attaining good conversion values in the MPV reaction of FUR [23,39–42] and Zr^{4+}-MOFs [25]. Recently, several authors have reported that the coexistence of acid and basic sites have a synergistic effect on the catalytic behavior in MPV processes, as observed for Al_2O_3 [25], ZrO_2 [21,23] and metal oxides obtained from hydrotalcites, like MgO/Al_2O_3 [43,44] and MgO/Fe_2O_3 [26].

In this context, several metal oxides such as, ZrO_2, Al_2O_3/ZrO_2 (with different Zr/Al molar ratio) and Al_2O_3 were synthesized by an easy and relatively inexpensive methodology as co-precipitation. Then, the obtained oxides were characterized by different physico-chemical techniques. The main objective of the present work was to evaluate the possible synergistic effect between Al_2O_3 and ZrO_2 in the MPV reaction of FUR into high-added value products as FOL, which is highly used in the synthesis of polymers [5]. Once the catalysts were tested, the best catalyst was selected to optimize the reaction conditions for attaining the maximum FOL yield. On the other hand, the present research also aimed to the analysis of the role of the acid and basic sites involved in the MPV process as well as the presence of H_2O in the reaction medium. Finally, in order to assess the sustainability of the catalysts, several reaction cycles were carried out for the Al_2O_3, ZrO_2 and Al_2O_3/ZrO_2 catalysts.

2. Materials and methods.

2.1. Synthesis of catalysts

The precursor salts used for the synthesis of catalysts were aluminum (III) nitrate nonahydrate, $Al(NO_3)_3{\cdot}9H_2O$ (98%) and zirconyl chloride octahydrate, $ZrOCl_2{\cdot}8H_2O$ (99%), supplied by Sigma-Aldrich. Ammonia (25-28% NH_3 basis) was supplied by Alfa Aesar.

Chemicals involved in the MPV reaction were: furfural (Sigma-Aldrich, 99%), 2-propanol (VWR, HPLC grade, 99.9%), used as sacrificing alcohol, and o-xylene (Sigma-Aldrich, 99.9%) employed as internal standard. The gases employed were He (Air Liquide, 99.99%), NH_3 (Air Liquid, 99.99%), CO_2 (Air Liquid, 99.99%), H_2 (Air Liquide, 99.999%) and N_2 (Air Liquide, 99.9999%).

2.2. Preparation of catalysts

Mixed Al-Zr oxide catalysts were synthesized by a co-precipitation method. In a typical procedure, the required amounts of $ZrOCl_2 \cdot 8H_2O$ and $Al(NO_3)_3 \cdot 9H_2O$ were dissolved in 200 mL of deionized water to obtain a final solution of these salts of 0.5M. The pH of the resulting solution was increased until 9 by adding dropwise an aqueous ammonia solution (25-28%), under vigorous stirring. The gel obtained under these conditions was aged at room temperature for 5 h. Then, it was filtered and washed with deionized water until a neutral pH. Later, solids were dried overnight at 80 ºC and, finally, calcined at 400 ºC (2 ºC min^{-1}), maintaining this temperature for 4 h to obtain the Al_2O_3-ZrO_2 catalysts.

The synthesized catalysts were labeled as Zr, Al and Zr_xAl_y, where Zr was the ZrO_2 catalyst, Al was the Al_2O_3 catalyst and Zr_xAl_y were the ZrO_2/Al_2O_3 catalysts where *x* and *y* indicated molar ratio between Zr and Al, respectively.

2.3. Characterization of the catalysts

The crystalline phases of catalysts were determined from their XRD patterns, using a PANalytical X'Pert PRO diffractometer, over a 2θ range with Bragg-Brentano geometry using the Cu Kα (1.5406 Å) radiation and a Ge-monochromator. The average crystallite size and the lattice strain were evaluated from the Williamson-Hall method, using the equation: $B \cos \theta = (K \lambda/D) + (2 \varepsilon \sin \theta)$, where θ is the Bragg angle, B is the full width at half maximum (FWHM) of the XRD peak, K is the Scherrer constant, λ is the wavelength of the X-ray and ε the lattice strain [45].

The catalyst morphology was studied by Transmission Electron Microscopy (TEM), using FEI Talos F200X equipment (Thermo Fisher Scientific). This equipment combines outstanding high-resolution S/TEM and TEM imaging with industry-leading energy dispersive X-ray spectroscopy (EDS) signal detection, and 3D chemical characterization with compositional mapping. The samples were dispersed in ethanol and a drop of the suspension was put on a Cu grid (300 mesh).

N_2 adsorption-desorption isotherms at -196 ºC were obtained by using an ASAP 2020 model of gas adsorption analyzer supplied for Micromeritics Inc. Prior to the measurements, samples were outgassed overnight at 110 ºC and 10^{-4} mbar. Micropore surface areas were obtained by de Boer's t-plot method [46]. The specific surface area

was determined by the Brunauer-Emmett-Teller equation (BET), using the adsorption data in the range of relative pressures at which conditions of linearity and considerations regarding the method were fulfilled and taking into account that the N_2 cross section is 16.2 $Å^2$ [47]. The pore size distribution was determined from the desorption branch of the isotherm using the Non-local Density Functional Theory (NLDFT) [48]. The total pore volume was calculated from adsorbed N_2 at $P/P_0 = 0.996$.

Acid and basic sites concentrations were determined by temperature-programmed desorption (TPD) analysis. On one hand, the amount of acid sites was determined by TPD of ammonia (NH_3-TPD). Each experiment was carried out using 0.08 g of catalyst. In a first step, the catalyst was cleaned using a He flow (40 mL min^{-1}) from room temperature to 550 ºC, with a heating rate of 10 ºC $min^{-1,}$ and maintaining this temperature for 15 min, and it was then cooled under the same conditions until 100 ºC. Later, the catalyst was saturated with pure NH_3 for 5 min. Subsequently, a He flow (40 mL min^{-1}) was passed to eliminate the physisorbed ammonia. Finally, ammonia desorption was carried out by heating the samples from 100 to 550 ºC, at a heating rate of 10 ºC min^{-1}. A thermal conductivity detector (TCD) quantified the desorbed ammonia. On the other hand, the amount of basic sites was quantified by the TPD of carbon dioxide (CO_2-TPD). In each analysis, 0.3 g of sample was pretreated under a He flow (40 mL min^{-1}) at 550 ºC for 15 min (10 ºC min^{-1}). The temperature was lowered to 100 ºC and a pure CO_2 stream (60 mL min^{-1}) was subsequently introduced into the reactor for 30 min. After removing physisorbed CO_2, CO_2-TPD was carried out between 100 and 550 ºC under a He flow (10 ºC min^{-1} and 30 mL min^{-1}) and the amount of CO_2 evolved was analyzed using a TCD detector.

DRIFT spectra of adsorbed pyridine were recorded on a VERTEX 70 spectrometer coupled with an external sample chamber that enables measurements under vacuum (Bruker). The samples were mixed with KBr and grounded prior to the measurement. Samples were dried in situ under vacuum (around $1.5 \cdot 10^{-3}$ mbar) for 1 h at 200 °C, and later cooled down to 40 °C in order to record the background spectra. The main measurement features were a spectral range from 1800 to 1200 cm^{-1}, 200 scans, and a resolution of 2 cm-1. Initially, the catalyst was put in direct contact with pyridine at 40 °C for 8 min. Analysis were obtained by heating the samples under vacuum (1-$5 \cdot 10^{-3}$ mbar) up to 40, 110 or 150 °C for 15 min.

A Physical Electronics PHI5700 spectrometer with non-monochromatic Mg Kα radiation (300 W, 15 kV and 1253.6 eV) with a multichannel detector was used to determinate the X-ray photoelectron spectra of the samples. These spectra were recorded in the constant pass energy mode at 39.35 eV using a 720 μm diameter analysis area. Charge referencing was measured against adventitious carbon (C 1 s at 284.8 eV). A PHI ACCESS ESCA-V6.0F software package was used for acquisition and data analysis. A Shirley-type background was subtracted from the signals. Recorded spectra were always fitted using Gaussian–Lorentzian curves in order more accurately to determine the binding energies of the different element core levels.

The metal content of catalysts, as well as the leaching of catalysts, was evaluated by ICP-OES on a Perkin Elmer spectrophotometer (Optima 7300DV). Previously, the samples were digested in an Anton Paar device (Multiwave 3000) by using HF.

2.4. Catalytic tests

The catalytic transfer hydrogenation was performed in glass pressure reactors with thread bushing (Ace, 15 mL). In each experiment, 0.1 g of catalyst was mixed with 50 mmol isopropanol, 1 mmol furfural and 0.1 mmol o-xylene as the internal standard. Prior to each experiment, this solution was sonicated and purged with He to avoid catalyst carbonation. The reaction was carried out in a silicone bath, between 1 and 6 h, at different reaction temperatures (90 - 130 ºC), being controlled with a thermocouple in direct contact with the silicone oil. Reaction products were microfiltered and analyzed by gas chromatography (Shimadzu GC model 14A), equipped with a Flame Ionization Detector and a CP-Wax 52 CB capillary column. Furfural conversion, selectivity and yield were calculated as follows:

$$\text{Conversion (\%)} = \frac{\text{mol of furfural converted}}{\text{mol of furfural fed}} \times 100$$

$$\text{Selectivity (\%)} = \frac{\text{mol of the product}}{\text{mol of furfural converted}} \times 100$$

$$\text{Yield (\%)} = \frac{\text{mol of the product}}{\text{mol of furfural fed}} \times 100$$

In order to comparatively evaluate the role of acid and basic sites involved in the MPV of FUR, pyridine or benzoic acid, which can interact with the acid and basic sites, respectively, were added into the reaction medium. Thus, the addition of benzoic acid

can block the basic sites, while the addition of pyridine can block the acid sites. The catalytic conditions described above were also used for these studies, but adding pyridine, benzoic acid or H_2O using the following molar ratio (FUR/catalyst mass ratio: 1, FUR/pyridine molar ratio: 0.75 or FUR/Benzoic acid molar ratio: 0.75 or FUR/H_2O molar ratio: 0.33). These ratios were selected to have an excess of these molecules in comparison to the amount of acid and/or basic sites.

3. Characterization of the catalysts

The crystalline phases present in the catalysts were studied by X-ray diffraction (Figure 1). Focusing on the Zr catalyst, the typical diffraction peaks of two crystalline ZrO_2 phases were observed, which were quantified by using a Rietveld analysis: 44% tetragonal ZrO_2 (2θ (º) = 30.3, 34.3, 35.2, 50.1, 51.3, 59.2, 60.1 and 62.3, PDF N. 04-013-0070) and 56% monoclinic ZrO_2 (2θ (º) = 24.2, 24.8, 28.2, 31.4, 33.9, 38.7, 40.8, 44.8, 49.1, 50.3, 51.2, 55.4, 62.8 and 65.5, PDF N. 00-065-0687). The Williamson-Hall method [45] provided average crystallite sizes very similar for both phases: 15.3 and 12.3 nm for tetrahedral and monoclinic ZrO_2, respectively.

On the other hand, Al_2O_3 (Al) exhibits broader diffraction peaks at 2θ (º) = 27.8, 37.8, 46.0, 48.8 and 65.8, ascribed to γ-Al_2O_3 (PDF N. 04-008-4096), with average particle size of 6.1 nm, lower than those observed for both ZrO_2 phases. In the case of the mixed oxides, Zr_xAl_y, defined diffraction peaks were not observed, so these are amorphous, or crystallite sizes are too small to be identified by the X-ray diffraction technique.

The catalyst morphology, as deduced from TEM micrographs (Figure 2), in all cases, consists of aggregates of small particles, where interparticle voids seem to generate a disorder porous structure. These data are in agreement with the low crystallinity inferred from XRD data (Figure 1). In spite of Zr catalyst showed the highest crystallite sizes, its morphology does not evidence clear differences with the rest of catalysts. The EDX analysis reveals that both Al and Zr species are well dispersed in the Zr_xAl_y catalysts. These data are in agreement with those obtained by other authors in Al_2O_3/ZrO_2 systems calcined at similar temperature [49]. These authors observed that these mixed metal oxides are homogeneously distributed, being formed by individual Al_2O_3 and ZrO_2 particles with a size of approximately 10 nm, discarding the formation of solid solutions [49].

Textural properties were determined from the N_2 adsorption-desorption isotherms at -196 ºC (Figure 3A). According to the IUPAC classification, these isotherms can be classified as Type IV, which are characteristic of many oxide gels and mesoporous adsorbents [50]. The hysteresis loops are Type H4, associated to the existence of micropores and small mesopores, such as zeolites, carbons or metal oxides [50].

The pore size distribution was determined by the DFT method [48] (Figure 3B). All catalysts display similar pore size distributions where it is noteworthy the presence of a first contribution between 1-2 nm and a second one located between 2 and 12 nm. Moreover, it can also be observed that micro- and mesoporosity increase with the Al content. In any case, catalysts exhibit a broad distribution of pore sizes.

The specific surface areas, determined from the BET equation [47], are compiled in Table 1. The data indicate that Zr is the catalyst with the lowest S_{BET} (101 m^2 g^{-1}), in agreement with the crystallinity degree (Figure 1 and 2), since the existence of bigger particles diminishes the proportion of voids between adjacent particles, leading to poorest textural properties. For the Zr_xAl_y catalysts, as the aluminum content increases, the specific surface area is higher, reaching the highest S_{BET} value (312 m^2 g^{-1}) for the Al catalyst, as a result of its higher microporosity (t-plot values) due to the presence of small interparticle voids. The pore volume is directly related to the micro- and mesoporosity of the catalyst, in such a way the Al catalyst also has both the highest micro and mesoporous volumes.

In addition, it has been reported in the literature that both acid and basic sites can be involved in the MPV reaction [12,30,44], so the next characterization step was to determine the acid-basic properties of catalysts. The total acidity was determined by NH_3-TPD (Table 2), revealing that the amount of acid sites was very high in most of cases, probably due to their high specific surface area (Table 1). Previously, similar acidity values to those obtained in the present work were reported after calcination of catalysts at low temperature (300-400 ºC) [49,51].

The acidity data demonstrate that the acidity increases with the Al content, from 489 μmol g^{-1} for the Zr catalyst up to 1115 μmol g^{-1} for Zr_5Al_5 catalyst. However, for materials with a higher Al content, the acidity does not increase (966 and 959 μmol g^{-1} for Zr_3Al_7 and Al catalysts, respectively). The NH_3-TPD profiles are similar for all materials, with a broad desorption band (Supplementary Information, Figure 1), which

would suggest that these metal oxides (Al and Zr catalysts) display acid sites with variable strength and that the formation of mixed metal oxides does not modify this strength. Additionally, the basicity of these materials was also evaluated from the CO_2-TPD (Table 2). It is noteworthy that the amount of basic sites is much lower than that of acid sites in all catalysts. Moreover, the strength of these basic sites is relatively weak, since CO_2 is desorbed below 300 ºC (Supplementary Information, Figure 2). Zr catalyst is the sample with the lowest quantity of basic sites, 4 μmol g^{-1}, whereas the progressive incorporation of Al causes an increase in the proportion of basic sites, attaining the highest value for the Zr_3Al_7 catalyst (39 μmol g^{-1}).

Taking into account that the type of acid sites plays an important role in the catalytic activity of the MPV reaction, FTIR spectra after pyridine adsorption after evacuating at different temperatures (40, 110 and 150 ºC) studies were carried out to discern between Lewis and Brønsted acid sites (LAS and BAS) (Figure 4). It is well known that the existence of LAS is demonstrated by bands about 1608 and 1444 cm^{-1} which are related to the 8a and 19b vibration modes of pyridine coordinated to LAS, respectively, which are detected in all cases [52]. However, the strength of these sites is different since the intensity of these bands considerably decreases after increasing the evacuation temperature for mixed oxides, being this decrease less pronounced for pure Zr and Al catalysts. Regarding BAS, two bands about 1630 and 1535 cm^{-1} are slightly detected for Zr catalyst after outgassing at 40 ºC which could be associated to the 8a and 19b vibration modes of pyridine coordinated to Brønsted acid sites [53]. However, these bands disappears after evacuation at higher temperatures for Zr catalyst and they are not observed for the rest of materials. Only in the case of Zr_3Al_7 catalyst, the peak at 1535 cm^{-1} is found for high outgassing temperatures (110 and 150 ºC), but it is not observed after evacuation at 40 ºC. Hence, these low intense peaks could be related to the oxidative breakdown of pyridine on strong Lewis acid sites giving rise to carbonaceous species [54] rather than BAS due to this peak was not detected after outgassing at 40 ºC and its intensity also grew with the evacuation temperature. Finally, another band at 1590 cm^{-1} is found in all cases after outgassing at 40 ºC which is related to the 8a vibration mode of pyridine bonded by hydrogen bond to the hydroxyl groups of the catalyst surface [55]. This band disappears after evacuation at higher temperatures except for Al catalyst, demonstrating that the interaction of pyridine with surface hydroxyl groups is stronger for this catalyst. Therefore, this serie of catalysts has shown

mostly LAS and, only in the case of Zr catalysts, very weak BAS were found. These data are in agreement with those reported for other authors in Zr-Al mixed oxides by pyridine adsorpion coupled to FTIR spectroscopy [51]. These authors observed the typical bands of pyridine associated to Lewis acid sites, while those ascribed to Brønsted acid sites were hardly detected [51]. In addition, the content of Lewis acid sites significantly enhanced with the addition of Al to ZrO_2, which is in agreement with results obtained from NH_3-TPD [51].

In order to get insights into the surface chemical composition of catalysts, XPS analysis was carried out (Table 3). The analysis of the Zr 3d core level spectra shows a contribution between 182.2 and 182.9 eV, assigned to Zr in ZrO_2 (Supplementary Information, Figure 3). Considering that Zr and Al species are well dispersed in the mixed metal oxides, as previously inferred from EDX analysis (Figure 2), the increase in the Zr binding energy when Al is incorporated could be caused by an increase in the positive charge of Zr atoms due to the higher electronegativity of Al in Zr-O-Al bonds, which can also increase the amount and strength of Lewis acid sites, as was reported previously in the literature [56,57]. In the same way, the Al 2p core level spectra also shows a band between 74.6 and 74.9 eV, which is ascribed to Al_2O_3 (Supplementary Information, Figure 3). In the case of O 1s region, the spectra also show a contribution, which evolves from 532.0 eV for the Zr catalyst to 531.4 eV for the Al catalyst, being attributed to O in metal oxides, in all cases (Supplementary Information, Figure 3). From these data, it can be inferred an increase in electronic density in the case of the Al_2O_3. This behavior will agree with the higher electronegativity of Al in comparison with Zr, in such a way that the electronic density on O atoms would be higher in the case of a Zr-O bond. On the other hand, the surface chemical composition of Zr_xAl_y catalysts (Table 3) points out that the Al/Zr molar ratio is very close to the theoretical values. This could be ascribed to the precipitation of both Zr and Al species under the same pH conditions, as well as the formation of ZrO_2 and Al_2O_3 particles that do not differ much in size, as observed in TEM micrographs (Figure 2), in spite of XRD data showed that ZrO_2 possesses a higher crystallinity (Figure 1).

The environment of Al atoms was studied by ^{27}Al NMR., since Al atoms can adopt different geometries, mainly octahedral, pentahedral and tetrahedral, with distinctive signals at -10-20 ppm (AlO_6), 30-40 ppm (AlO_5) and 50-85 ppm (AlO_4) [58]. Data

reported in Figure 5 pointed out that the Al catalyst mainly displays Al species in octahedral environment, about 83%, and a lower proportion of tetrahedral AlO_4 species (17%). The incorporation of Zr in Zr_xAl_y catalysts progressive decreases the intensity of band associated to octahedral AlO_6 species, and concomitantly increase the contribution of AlO_4 and AlO_5 species. In this sense, previous research have reported that tetra- and penta-coordinated Al species are at least partially located on the γ-alumina surface. These coordination sites are considered as potential Lewis acid sites [59], which are required for the catalytic transfer of hydrogen to reduce FUR molecules [12]. Similar data were also reported by Liu and Truitt from DRIFT spectra, obtained after pyridine adsorption, where Lewis acid sites were assigned to three-, four-, and five-coordinated Al^{3+} ions [60]. On the other hand, it has been reported in the literature that Zr-species interact with pyridine through their Lewis acidic-basic $Zr^{4+}O^{2-}$ pair [12,61].

4. Catalytic results

After the physico-chemical characterization of catalysts, they were evaluated as heterogeneous catalysts in the reduction of FUR to high value-added products by catalytic transfer hydrogenation.

The first catalytic study was carried out at 110 ºC (Figure 6 and Supplementary Information, Table 1), under similar experimental conditions to those previously reported by several authors [23,39]. In the absence of catalyst, no activity was detected in the MPV reaction of FUR. However, all the catalysts prepared in the present work are active (Figure 6A), with FUR conversion values increasing directly with the reaction time. The higher activity is shown by mixed Zr_xAl_y oxides, attaining the highest FUR conversion (96%) with the Zr_5Al_5 catalyst, after 6 h at 110 ºC, which was the catalyst with the highest acidity. These data are better than those reported in the literature under similar experimental conditions [23,25,39]. The excellent catalytic activity could be ascribed to the presence of ZrO_2 or Al_2O_3 nanoparticles with high surface area, as well as high amount of basic and mainly acid sites (Table 2). ^{27}Al NMR also indicated that the increase in Zr in the Zr_xAl_y catalysts favored the formation of tetrahedral and, mainly, pentahedral aluminum species [59,60], which seem to be responsible of the existence of Lewis acid sites and, therefore, favor the CTH reaction of FUR [12,59,60].

Single metal oxides (Al and Zr) are less active than mixed Zr_xAl_y oxides. Thus, after 6 h of reaction, Al and Zr catalysts reach FUR conversions of 77 and 68%, respectively,

which are similar to those previously reported for, either synthesized or commercial, Al_2O_3 and ZrO_2 catalysts. Thus, a commercial alumina attained a FUR conversion of 82% [25], while ZrO_2 gave rise to a value below 70% [23] under similar catalytic conditions to that reported in the present work. The Al catalyst showed a FUR conversion higher than Zr catalyst throughout the reaction time, which could be explained by taking into account its higher amount of available active sites (acidic and basic) in the Al catalyst. From textural properties (Table 1), it was observed that the surface area increases as the aluminum amount does. This fact could imply that the catalytic activity should increase for the catalyst with a higher aluminum content, since the strength of acid sites is similar in all catalysts (Table 2). However, these catalysts also display high microporosity, so it is plausible that bulkier molecule as FUR cannot access to all active sites involved in the MPV reaction, in such a way that lower conversion values were obtained than those expected for Zr_3Al_7 and Al catalysts. In addition, acid sites within narrower pores are more prone to be deactivated by the formation of carbonaceous deposits.

With regard to the selectivity pattern (Figure 6B), both Al and Zr_xAl_y catalysts are very selective towards FOL [12,20], with the highest FOL yield (93%) attained with the Zr_5Al_5 catalyst, after 5 h at 110 ºC, probably due to its highest amount of acid sites. In the case of the Zr catalyst, in spite of being less active than the rest of catalysts, consecutive reactions are observed (Figure 6C). Thus, in a first step, FUR is reduced through CTH to FOL. In spite of it has been reported in the literature that Zr catalyst must display a high proportion of Lewis acid sites, FOL tends to undergo slightly etherification [61]. This reaction is catalyzed through small proportion of Brønsted sites of ZrO_2, (Zr-OH-Zr) (Figure 4) [54], and FOL and the sacrificing alcohol react to produce i-propyl furfuryl ether (iPFE), reaching a yield about 10% after 6 h of reaction at 110 ºC. Alkylfurfuryl ethers are also considered valuable products, since these can be used as diesel additives due to their high cetane number [62,63], as well as flavoring ingredient to provide a nutty or coffee taste to drinks and foods [64].

The etherification reaction of FOL with alcohols is governed by Brønsted acid sites, as inferred from the high conversion values reached when a typical Brønsted acid catalyst, like a cationic exchange resin as Amberlyst-15, was used. [65]. These authors pointed out that Brønsted acid sites favor the generation of a better leaving group, so the

etherification reaction must take place through a S_N1 mechanism [65,66]. On the other hand, other authors have reported that the etherification reaction can also take place through Lewis acid sites, although a higher reaction temperature was required [67,68]. It was also pointed out that the hydroxyl group of FOL donated its loan pair of electrons to the Lewis acid sites associated with Zr species to generate an oxonium ion ($R\text{-}O^+$). Then, this group might be attracted by the alcohol to form alkyl furfuryl ethers [67].

In the case of mixed Zr_xAl_y oxides, the etherification reaction is negligible. Considering that the NH_3-TPD profile is similar in all cases and that the amount of acid centers does not seem to be related to the etherification reaction, it is expected that the reaction is governed by the Lewis acid sites such that only the catalytic transfer of hydrogen takes place.

The small proportion of Brønsted acid sites in the case of the Zr catalyst (Figure 4) can also facilitate the opening ring of iPFE to obtain i-propyl levulinate (iPL), although its yield is not very high, not exceeding 8% in the best case. The furan ring opening occurs through the attach of H_2O, coming from the etherification reaction, to form dienol intermediate, which would further transformed to butyl levulinates via the keto-enolisomerisation [66,67]. Alkyl levulinates present interesting physicochemical properties, being used as specialty chemicals in chemical and petrochemical industries [69]. Several authors have reported that stronger reaction conditions are required to obtain alkyl levulinates, even γ-valerolactone (GVL) from FUR, since it is necessary the coexistence of Brønsted and Lewis acid sites and high temperature ($T > 140$ ºC) and long reaction times ($t > 12$ h) for the cyclation of the alkyl levulinate into GVL [40,70,71]. If the reaction starts from FOL, Lewis acid sites are not required, so the reaction takes place in shorter reaction times and lower reaction temperature [72,73].

The use of more severe experimental conditions improves the catalytic activity, although an adverse effect in yields due to the acid sites favors the polymerization of FUR and FOL, thus causing the blocking of active sites, is also observed [74]. Under the more severe conditions, the small amount of Brønsted acidity (Figure 4) [75] are responsible for the alcoholysis reaction to give rise to iPFE and iPL [74]. In the case of the Zr_xAl_y, the absence of Brønsted acid sites (Figure 4) inhibits the etherification and alcoholysis products under the catalytic conditions reported in the present research.

As Zr_5Al_5 was the mixed metal oxide catalyst with the highest FUR conversion and FOL yield, this catalyst was compared with Al and Zr catalysts in a more detailed study to elucidate the influence of other experimental variables. In this sense, the influence of the reaction temperature on the catalytic behavior was also evaluated (Figure 7 and Supplementary Information, Table 2). The FUR conversion with Zr_5Al_5 increases directly with the reaction temperature (Figure 7A), and, at 90 ºC, FUR conversion improves linearly along the reaction time, obtaining a value of 69% after 6 h of reaction. The use of higher reaction temperature gives rise to a faster FUR conversion, in such a way that it is possible to reach a conversion of 93% after only 2h of reaction at 130 ºC. The modification of the reaction temperature does not favor the formation of other reaction products, FOL being the only product detected. The increase of the temperature only accelerates the reaction, reaching a maximum FOL yield of 89% after only 2 h of reaction at 130 ºC (Figure 7B). This fact would demonstrate that CTH is the only reaction catalyzed by these mixed metal oxides (Zr_xAl_y) under the studied temperature range (90-130 °C), discarding other side reactions.

In the case of the Al catalyst (Figure 8A and Supplementary Information, Table 2), the effect of the reaction temperature follows the same trend to that observed for Zr_5Al_5, where the FUR conversion directly increases with the temperature. However, a longer reaction time is required to reach an almost full FUR conversion, as a consequence of the lower proportion of active sites in comparison to Zr_5Al_5 catalyst, since it is needed 5 h at 130 °C to achieve a conversion of 95%. Similarly to Zr_5Al_5 catalyst, FOL is the only reaction product for the Al catalyst (Figure 8B) in this temperature range, which is in agreement with data reported in the literature for Al_2O_3 catalysts [25]. This fact implies the absence of side reactions when Al catalyst was used in the temperature range (90-130 ºC). Under these conditions, a maximum FOL yield of 89% after 5 h of reaction at 130 ºC was attained with this catalyst. Therefore, longer reaction times are required to obtain similar FOL yields with the Al catalyst, compared with the Zr_5Al_5 catalyst.

For the Zr catalyst (Figure 9 and Supplementary Information, Table 2), FUR conversion resembles that exhibited by the Al catalyst, also requiring longer reaction time to attain high FUR conversion (93% after 6 h of reaction at 130 ºC) due to its low amount of active sites. The major product was FOL, so the reaction mainly takes place via CTH,

although other products such as iPFE and iPL were also detected for higher reaction temperatures. These products, coming from the etherification and alcoholysis reactions of FOL, are favored at higher temperature [70,71].

In order to evaluate the potential activity of acid and basic sites involved in the MPV reactions, the amount of FUR converted by acid/basic sites and mass of catalyst was calculated (Figure 10). The analysis of the FUR conversion per acid sites (Figure 10A) show that all the catalysts follow the same trend after the first hour of reaction, but, at longer reaction time, FUR converted tend to a plateau for Al and Zr_5Al_5 catalysts, while Zr catalyst maintains a quasi-linear FUR conversion along the six hours of reactions, being the most active catalyst per gram and per active site. A similar pattern was observed when FUR conversion was expressed per basic sites (Figure 10B). After 1 h of reaction, all catalyst displays a similar activity, in agreement with the TPD profiles (Supplementary Information, Figures 1 and 2), since the strength of basic active sites is very similar in all cases. The decay of the amount of FUR converted along the reaction time for Al and Zr_5Al_5 could be ascribed to its textural properties, due to these catalysts display high microporosity, as inferred from t-plots, which could be easily blocked by the formation of carbonaceous deposits. In this sense, previous research carried out under similar experimental conditions, using Zr-doped porous silicas, demonstrated that high microporous catalysts are more prone of blocking their pores throughout the MPV reaction [23]. On the other hand, these authors also found the formation of carbonaceous deposits [25,26] Thus, an increase in the carbon content on the catalyst surface after the reaction, as determined by XPS, was found for heterogeneous acid catalysts, such as Al_2O_3 [25] as well as catalysts with higher proportion of basic sites as $MgO\text{-}Fe_2O_3$ [26] by XPS reported an increase of the carbon content in its surface after the reaction.

As the optimization of experimental parameters, such as sacrificing alcohol, furfural/alcohol molar ratio and catalyst loading of catalyst, was carried out in a previous work [23], the next tests were focused on the analysis of the catalyst stability. Thus, catalysts were studied during four catalytic runs under mild conditions, 3 h of reaction at 110 ºC (Figure 11). In all cases, it is noteworthy a progressive decay of FUR conversion after each run (Figure 11A), which is more pronounced in the case of the most active Zr_5Al_5 catalyst, since FUR conversion decreases from 84% after the 1st run

to 56% after 4th run. The less active catalyst Al was also deactivated, from 62% to 43%, while in the case of the Zr catalyst, whose FUR conversion is the lowest of all the catalysts studied, it deactivates less after each execution. In this sense, it has been previously reported that the presence of a high amount of active sites can favor the formation of carbonaceous deposits coming from the polymerization of FUR and FOL [70], whose strong interaction with the active sites decreases their available number [23]. The analysis of the catalyst surface by XPS, after 4th cycle, did not show changes in the contributions of O 1s, Zr 3d or Al 2p core level spectra although their atomic concentrations decreases in all cases (Supplementary Information, Figures 4). However, it is noteworthy an increase in the surface carbon content, which is directly related to the catalytic activity, since the Zr_5Al_5 catalyst shows a carbon content of 18.2%, while Al and Zr catalysts display 16.3 and 15.5%, respectively. This appearance of a new contribution about 289 eV assigned to -C=O confirms that FUR must interact strongly with the acid sites promoting the its polymerization. On the other hand, the deactivation by leaching must be discarded due to Al and/or Zr content, determined in the reaction medium after the catalytic test by ICP-OES, was < 0.01% for Al, Zr and Zr_5Al_5 catalysts after the 1st and 4th cycles.

However, other authors have reported that basic sites can also play an important role in the catalyst deactivation due to the formation of alkoxides from the sacrificing alcohol, which are prone to interact with basic sites [26,76]. In fact, the regeneration of the catalyst with strong basic sites is very complicated, since the calcination of these catalysts with adsorbed alkoxides form CO_2 that can block strong basic sites. In the present research, the decay of the FUR conversion after several cycles is lower than that shown in other catalysts with higher amount and stronger basic sites [26,76], so the deactivation should only be ascribed to the formation of carbonaceous deposits, which block the active sites and the microporous structure of catalysts. Considering these premises, the regeneration by calcination seems to be the more appropriate strategy to reactivate the catalyst, as was reported for Zr-doped mesoporous silicas used in this MPV catalytic process [21,23,25]. Thus, the thermal treatment of used catalysts allows attaining FUR conversions slightly lower than those achieved after the first cycle. This slight decrease in FUR conversion can be ascribed to the sintering of the active sites involved in the CTH reaction due to the combustion of the carbonaceous deposits strongly adsorbed on the catalyst surface takes place through an exothermic process,

which can cause the agglomeration of particles. In all cases, FOL was the only product in Al and Zr_5Al_5 catalyst and the main product for the Zr catalyst (the other products appear in Fig. 8). This pattern hardly changes after several reaction cycles in the case of Al and Zr_5Al_5 catalysts. In the case of the Zr catalyst, the small proportions of iPFE and iPL disappear after the first cycle.

Taking into account that CTH reaction involves both acid and basic sites, the next tests aimed to evaluate the role of these acid and/or basic centers in the catalytic reaction. In order to observe more clearly the differences between the catalytic tests, mild experimental conditions (110 ºC) were used. In a first study, a basic molecule, such as pyridine, was added in excess to the reaction medium to block all acid sites of Zr_5Al_5 catalyst. This causes a strong decrease in FUR conversion, from 95% to 46%, which would indicate that acid sites are required for the CTH reaction of FUR (Figure 12). This data could be expected, since the amount of acid sites are predominant in this catalyst.

In the next study, an acid molecule, such as benzoic acid, was also used in excess to neutralize basic sites of the Zr_5Al_5 catalyst. The catalytic results, shown in Figure 12, reveal that the blocking of basic sites is less relevant for the catalytic process in comparison with acid sites blocked with pyridine, which could be a consequence of the higher proportion of acid sites (Table 2). In previous research carried out using MgO/Fe_2O_3 catalysts for the CTH of FUR [26], where the amount and strength of basic sites were higher in comparison to the catalysts reported in the present work, the blockage of basic sites led to FUR conversion almost negligible. Therefore, it could be concluded that the amount of basic sites and, mainly their strength, exerts important role in the CTH reaction. However, the low amount and strength of basic sites of Zr, Al and Zr_xAl_y catalysts pointed out that a less relevant role in the CTH reaction of FUR is played in the present work. Thus, it seems clear that the acid sites are the active centers of these catalysts, which are involved in the MPV reaction of FUR.

Taking into account the growing interest of one-pot reactions to obtain FOL or another valuable products from their respective sugar monomer (xylose), the influence of H_2O in the reaction medium was also evaluated, since three water molecules are generated in the dehydration of xylose into FUR (Figure 12). Thus, a H_2O/FUR molar ratio of 3 was added in the reaction medium to analyze the role of H_2O in the CTH reaction. The

catalytic data show how the presence of H_2O has an adverse effect in the catalytic behavior, since FUR conversion decays from 96% to 59% after 6 h of reaction at 110 ºC. In this sense, the presence of H_2O can block the Lewis acid sites involved in the CTH reaction, and thus, for instance, they can be transformed into Brønsted acid sites, which could favor consecutive reactions, such as the etherification of FOL. However, these products are not detected in no case, so that the addition of H_2O seems to have an inhibitory role in the catalytic behavior.

In order to rule out the influence of Brønsted acidity on the MPV reaction of FUR, Amberlyst-15, a typical Brønsted acid catalyst, was tested under similar experimental conditions. However, this catalyst is inactive in the CTH process, although it was active in the dehydration of the sacrificing alcohol [25,77].

The present catalytic results have demonstrated that FUR can be converted to FOL by using solid acid catalysts based on mixed ZrO_2/Al_2O_3, with isopropanol as hydrogen donor alcohol. However, this secondary alcohol is miscible with water, thus avoiding its application for the dehydration of xylose, coming from the hydrolysis of hemicellulose, in a biphasic water: organic solvent system, to produce FUR, which could be subsequently reduced to FOL in the presence of isopropanol. In this sense, a study is being carried out to use long hydrocarbon chain alcohols, less miscible with water, to perform the one-pot conversion of xylose to furfuryl alcohol.

5. Conclusions

Al_2O_3, ZrO_2 and ZrO_2/Al_2O_3 with different Zr/Al molar ratio have been synthesized by co-precipitation method in basic medium and subsequent calcination. The characterization of these catalysts reveal the Al_2O_3 and ZrO_2/Al_2O_3 catalyst display a small crystal size and high specific surface area, which provides a wide dispersion of a high proportion of acid sites. As the Zr content increases, the catalysts have lower surface areas due to a decay in their microporosity. This fact supposes a lower amount of acid sites.

The catalytic tests revealed that the Zr_5Al_5 catalyst was the most active in the CTH reaction of FUR, reaching a highest FUR conversion of 95% with a yield towards FOL above 90% after 5h of reaction at 130 °C so the coexistence of ZrO_2 and Al_2O_3 exerts a synergetic effect, as suggested the increase in the amount of acid sites for these

catalysts. Both Al_2O_3 and ZrO_2/Al_2O_3 are selective to FOL in such a way that these catalysts only promote the CTH reaction. However, ZrO_2 catalyst shows, together with FOL, it is also observed iPFE and iPL such that CTH and the etherification reaction coexist under the reaction conditions reported in this research.

The analysis of the blockage of acid and basic sites revealed acid sites have a predominant role in the catalytic activity due to their higher proportion in comparison to basic sites. These catalysts suffer a progressive deactivation after each run, although it can be regenerated after thermal treatment, requiring milder conditions than those catalysts with a high proportion of basic sites.

Credit authors statement:

Cristina García-Sancho: Investigation, Data curation, Writing - Review & Editing

Carmem Pilar Jiménez Gómez: Investigation, Data curation, Writing - Original Draft, Visualization

Nerea Viar Antuñano: Investigation, Data curation

Juan Antonio Cecilia: Conceptualization, Methodology, Data curation, Writing - Original Draft, Writing - Review & Editing, Visualization, Supervision

Ramón Moreno Tost: Data curation, Writing - Review & Editing

Josefa M. Mérida-Robles: Conceptualization, Writing - Original Draft, Writing - Review & Editing, Supervision

Jesús Requies: Data curation, Writing - Review & Editing, Supervision

Pedro Maireles-Torres: Methodology, Resources, Investigation, Writing - Original Draft, Writing - Review & Editing, Supervision, Project administration, Funding acquisition

Declaration of interests

The authors declare that they have no known competing financial interests or personal relationships that could have appeared to influence the work reported in this paper.

Acknowledgments

The authors are grateful to financial support from the Spanish Ministry of Innovation, Science and Universities (Projects RTI2018-94918-B-C43 and RTI2018-094918-B-C44) and FEDER (European Union) funds. J.A.C. and C.G.S. thank University of Malaga for contracts of PhD incorporation. R.M.T. thanks to the Spanish Ministry of Economy and Competitiveness (IEDI2016-00743) for the financial support within the I3 program.

References

[1] G.W. Huber, S. Iborra, A. Corma, Chem. Rev. 106 (2006) 4044–4098.

[2] F. Delbecq, Y. Wang, A. Muralidhara, K.E. El Ouardi, G. Marlair, C. Len, Front. Chem. 6 (2018) 146–175.

[3] K.J. Zeitsch, The Chemistry and Technology of Furfural and Its Many By-Products, Elsevier, Amsterdam. The Netherlands, 2000.

[4] K. Yan, G. Wu, T. Lafleur, C. Jarvis, Renew. Sustain. Energy Rev. 38 (2014) 663–676.

[5] J.B. Barr, S.B. Wallon, J. Appl. Polym. Sci. 15 (1971) 1079–1090.

[6] R. Mariscal, P. Maireles-Torres, M. Ojeda, I. Sádaba, M. López Granados, Energy Environ. Sci. 9 (2016) 1144–1189.

[7] S. Sitthisa, D.E. Resasco, Catal. Letters 141 (2011) 784–791.

[8] C.P. Jiménez-Gómez, J.A. Cecilia, C. García-Sancho, R. Moreno-Tost, P. Maireles-Torres, ACS Sustain. Chem. Eng. 7 (2019) 7676–7685.

[9] C.P. Jiménez-Gómez, J.A. Cecilia, R. Moreno-Tost, P. Maireles-Torres, ChemSusChem 10 (2017) 1448–1459.

[10] C.P. Jiménez-Gómez, J.A. Cecilia, F.I. Franco-Duro, M. Pozo, R. Moreno-Tost, P. Maireles-Torres, Mol. Catal. 455 (2018) 121–131.

[11] B.M. Nagaraja, A.H. Padmasri, B. David Raju, K.S. Rama Rao, J. Mol. Catal. A Chem. 265 (2007) 90–97.

[12] M.J. Gilkey, B. Xu, ACS Catal. 6 (2016) 1420–1436.

[13] H. Meerwein, R. Schmidt, Ann. Der Chemie 444 (1925) 221–238.

[14] M. Verley, Bull. Soc. Chim. Fr. 37 (1925) 871–874.

[15] W. Ponndorf, Zeitschrift Für Angew. Chemie 39 (1926) 138–143.

[16] M. Boronat, A. Corma, M. Renz, J. Phys. Chem. B 110 (2006) 21168–21174.

[17] B. Uysal, B.S. Oksal, J. Chem. Sci. 123 (2011) 681–685.

[18] M. Normand, E. Kirillov, T. Roisnel, J.F. Carpentier, Organometallics 31 (2012) 5511–5519.

[19] E.J. Campbell, H. Zhou, S.B.T. Nguyen, Org. Lett. 3 (2001) 2391–2393.

[20] M. Chia, J.A. Dumesic, Chem. Commun. 47 (2011) 12233–12235.

[21] T. Komanoya, K. Nakajima, M. Kitano, M. Hara, J. Phys. Chem. C 119 (2015) 26540–26546.

[22] J.F. Miñambres, M.A. Aramendía, A. Marinas, J.M. Marinas, F.J. Urbano, J. Mol. Catal. A Chem. 338 (2011) 121–129.

[23] R. López-Asensio, C.P.J. Gómez, C.G. Sancho, R. Moreno-Tost, J.A. Cecilia, P. Maireles-Torres, Int. J. Mol. Sci. 20 (2019) 828–850.

[24] G. Chuah, S. Jaenicke, Y. Zhu, S. Liu, Curr. Org. Chem. 10 (2006) 1639–1654.

[25] R. López-Asensio, J.A. Cecilia, C.P. Jiménez-Gómez, C. García-Sancho, R. Moreno-Tost, P. Maireles-Torres, Appl. Catal. A Gen. 556 (2018) 1–9.

[26] R. Maderuelo-Solera, R. López-Asensio, J.A. Cecilia, C.P. Jiménez-Gómez, C. García-Sancho, R. Moreno-Tost, P. Maireles-Torres, Appl. Clay Sci. 183 (2019) 105351–105363.

[27] F. Li, S. Jiang, J. Huang, Y. Wang, S. Lu, C. Li, New J. Chem. 44 (2020) 478–486.

[28] M. Ma, P. Hou, P. Zhang, J. Cao, H. Liu, H. Yue, G. Tian, S. Feng, Appl. Catal. A Gen. 602 (2020) 117709.

[29] H. Heidari, M. Abedini, A. Nemati, M.M. Amini, Catal. Letters 130 (2009) 266–270.

[30] M.A. Aramendía, V. Borau, C. Jiménez, J.M. Marinas, J.R. Ruiz, F.J. Urbano, Appl. Catal. A Gen. 244 (2003) 207–215.

[31] A. Ramanathan, M. Carmen Castro Villalobos, C. Kwakernaak, S. Telalovic, U. Hanefeld, Chem. - A Eur. J. 14 (2008) 961–972.

[32] F. Gonell, M. Boronat, A. Corma, Catal. Sci. Technol. 7 (2017) 2865–2873.

[33] A. Corma, M.E. Domine, L. Nemeth, S. Valencia, J. Am. Chem. Soc. 124 (2002) 3194–3195.

[34] M.M. Antunes, S. Lima, P. Neves, A.L. Magalhães, E. Fazio, A. Fernandes, F. Neri, C.M. Silva, S.M. Rocha, M.F. Ribeiro, M. Pillinger, A. Urakawa, A.A. Valente, J. Catal. 329 (2015) 522–537.

[35] H.P. Winoto, B.S. Ahn, J. Jae, J. Ind. Eng. Chem. 40 (2016) 62–71.

[36] N.O. Popovych, P.I. Kyriienko, Y. Millot, L. Valentin, J. Gurgul, R.P. Socha, J. Żukrowski, S.O. Soloviev, S. Dzwigaj, Microporous Mesoporous Mater. 268 (2018) 178–188.

[37] H.Y. Luo, D.F. Consoli, W.R. Gunther, Y. Román-Leshkov, J. Catal. 320 (2014) 198–207.

[38] M. Koehle, R.F. Lobo, Catal. Sci. Technol. 6 (2016) 3018–3026.

[39] J. Iglesias, J.A. Melero, G. Morales, J. Moreno, Y. Segura, M. Paniagua, A. Cambra, B. Hernández, Catalysts 5 (2015) 1911–1927.

[40] J. Iglesias, J.A. Melero, G. Morales, M. Paniagua, B. Hernández, A. Osatiashtiani, A.F. Lee, K. Wilson, Catal. Sci. Technol. 8 (2018) 4485–4493.

[41] J. Zhang, K. Dong, W. Luo, H. Guan, ACS Omega 3 (2018) 6206–6216.

[42] J. Zhang, Y. Liu, S. Yang, J. Wei, L. He, L. Peng, X. Tang, Y. Ni, ACS Sustain. Chem. Eng. 8 (2020) 5584–5594.

[43] M.A. Aramendía, V. Borau, C. Jiménez, J.M. Marinas, J.R. Ruiz, F.J. Urbano, Appl. Catal. A Gen. 255 (2003) 301–308.

[44] Z. Xiao, Mol. Catal. 436 (2017) 1–9.

[45] G.K. Williamson, W.H. Hall, Acta Metall. 1 (1953) 22–31.

[46] B.C. Lippens, J.H. de Boer, J. Catal. 4 (1965) 319–323.

[47] S. Brunauer, P.H. Emmett, E. Teller, J. Am. Chem. Soc. 60 (1938) 309–319.

[48] J. Landers, G.Y. Gor, A. V. Neimark, Colloids Surfaces A Physicochem. Eng. Asp. 437 (2013) 3–32.

[49] J. He, H. Li, A. Riisager, S. Yang, ChemCatChem 10 (2018) 430–438.

[50] M. Thommes, K. Kaneko, A. V. Neimark, J.P. Olivier, F. Rodriguez-Reinoso, J. Rouquerol, K.S.W. Sing, Pure Appl. Chem. 87 (2015) 1051–1069.

[51] J. He, H. Li, Y.M. Lu, Y.X. Liu, Z.B. Wu, D.Y. Hu, S. Yang, Appl. Catal. A Gen. 510 (2016) 11–19.

[52] J.M.R. Gallo, C. Bisio, G. Gatti, L. Marchese, H.O. Pastore, Langmuir 26 (2010) 5791–5800.

[53] P. Carniti, A. Gervasini, F. Bossola, V. Dal Santo, Appl. Catal. B Environ. 193 (2016) 93–102.

[54] M.I. Zaki, M.A. Hasan, F.A. Al-sagheer, L. Pasupulety, Colloids and Surfaces 190 (2001) 261–274.

[55] A. Ramírez, B.L. Lopez, L. Sierra, J. Phys. Chem. B 107 (2003) 9275–9280.

[56] C. García-Sancho, R. Moreno-Tost, J. Mérida-Robles, J. Santamaría-González, A. Jiménez-López, P. Maireles-Torres, Appl. Catal. A Gen. 433–434 (2012) 179–187.

[57] P. Salas, J.A. Wang, H. Armendariz, C. Angeles-Chavez, L.F. Chen, Mater. Chem. Phys. 114 (2009) 139–144.

[58] D. Engelhardt, G, & Michel, High-Resolution Solid-State NMR of Silicates and Zeolites, John Willey and son. Chichester, United States, 1987.

[59] D. Coster, A.L. Blumenfeld, J.J. Fripiat, J. Phys. Chem. 98 (1994) 6201–6211.

[60] X. Liu, R.E. Truitt, J. Am. Chem. Soc. 119 (1997) 9856–9860.

[61] F. Ouyang, A. Nakayama, K. Tabada, E. Suzuki, J. Phys. Chem. B 104 (2000) 2012–2018.

[62] E. de Jong, T. Vijlbrief, R. Hijkoop, G.J.M. Gruter, J.C. van der Waal, Biomass and Bioenergy 36 (2012) 151–159.

[63] G. Li, N. Li, Z. Wang, C. Li, A. Wang, X. Wang, Y. Cong, T. Zhang, ChemSusChem 5 (2012) 1958–1966.

[64] S. Yang, Y. Hao, J. Wang, H. Wang, Y. Zheng, H. Tian, Y. Liu, B. Sun, Sci. Rep. 7 (2017) 12954.

[65] E.R. Sacia, M. Balakrishnan, A.T. Bell, J. Catal. 313 (2014) 70–79.

[66] D. Song, S. An, B. Lu, Y. Guo, J. Leng, Appl. Catal. B Environ. 179 (2015) 445–457.

[67] B.S. Rao, P.K. Kumari, D. Dhanalakshmi, N. Lingaiah, Mol. Catal. 427 (2017) 80–86.

[68] S.R. B., K.K. P., D.L. D., N. Lingaiah, Catal. Today 309 (2018) 269–275.

[69] A. Démolis, N. Essayem, F. Rataboul, ACS Sustain. Chem. Eng. 2 (2014) 1338–1352.

[70] M.A. Mellmer, J.M.R. Gallo, D. Martin Alonso, J.A. Dumesic, ACS Catal. 5 (2015) 3354–3359.

[71] P. Neves, S. Lima, M. Pillinger, S.M. Rocha, J. Rocha, A.A. Valente, Catal. Today 218–219 (2013) 76–84.

[72] A.M. Hengne, S.B. Kamble, C. V. Rode, Green Chem. 15 (2013) 2540–2547.

[73] D.R. Chaffey, T.E. Davies, S.H. Taylor, A.E. Graham, ACS Sustain. Chem. Eng. 6 (2018) 4996–5002.

[74] J.P. Lange, W.D. van de Graaf, R.J. Haan, ChemSusChem 2 (2009) 437–441.

[75] G. Busca, Catal. Today 41 (1998) 191–206.

[76] M.S. Gyngazova, L. Grazia, A. Lolli, G. Innocenti, T. Tabanelli, M. Mella, S. Albonetti, F. Cavani, J. Catal. 372 (2019) 61–73.

[77] N.W. Cant, L.H. Little, Nature 211 (1966) 69–70.

List of captions

Figure 1. XRD diffractograms of Zr, Zr_xAl_y and Al catalysts.

Figure 2. S-TEM micrographs of the Zr and Al catalysts and mixed Zr_xAl_y catalysts.

Figure 3. N_2 adsorption-desorption isotherms at -196 ºC (A) and pore size distribution determined by DFT method (B) of Zr, Zr_xAl_y and Al catalysts.

Figure 4. FTIR spectra of adsorbed pyridine of Zr, Zr_xAl_y and Al catalysts.

Figure 5. ^{27}Al MAS NMR spectra of Zr_xAl_y and Al catalysts.

Figure 6. FUR conversion (A) and FOL yield (B) in the CTH reaction of furfural using Zr, Zr_xAl_y and Al catalysts. Detailed conversion and yield of Zr catalyst in the CTH reaction of furfural (C). (Experimental conditions: 110 ºC, 0.1 g of catalyst, 2-propanol/FUR molar ratio: 50, FUR/catalyst mass ratio: 1).

Figure 7. FUR conversion (A) and FOL yield in the CTH reaction of furfural (B) for Zr_5Al_5 catalyst. (Experimental conditions: 0.1 g of catalyst, 2-propanol/FUR molar ratio: 50, FUR/catalyst mass ratio: 1).

Figure 8. FUR conversion (A) and FOL yield (B) in the CTH reaction of furfural for Al catalyst. (Experimental conditions: 0.1 g of catalyst, 2-propanol/FUR molar ratio: 50, FUR/catalyst mass ratio: 1).

Figure 9. FUR conversion (A), FOL yield (B), iPFE yield (C) and iPL yield (D) in the CTH reaction of furfural for Zr catalyst. (Experimental conditions: 0.1 g of catalyst, 2-propanol/FUR molar ratio: 50, FUR/catalyst mass ratio: 1).

Figure 10. FUR conversion per gram of catalyst and acid site (A) or basic site (B) for Zr, Zr_5Al_5 and Al catalysts. (Experimental conditions: 3000 μmol of FUR, 2-propanol/FUR molar ratio: 50 and 1000 μmol of acid or basic sites).

Figure 11. Furfural conversion (A) and furfuryl alcohol yield (B) for Zr_5Al_5, Al and Zr catalysts after 4 cycles and after the regeneration treatment at 500 ºC for 2 hours. (Experimental conditions: 0.1 g of catalyst, temperature reaction: 110 °C, reaction time: 3 h, 2-propanol/FUR molar ratio: 50, FUR/catalyst mass ratio: 1).

Figure 12. Influence of the addition of acid, basic molecules and H_2O on the catalytic performance of the Zr_5Al_5 catalyst. (Experimental conditions: 0.1 g of catalyst, reaction temperature: 110 ºC, 2-propanol/FUR molar ratio: 50, FUR/catalyst mass ratio: 1, FUR/pyridine molar ratio: 0.75 or FUR/Benzoic acid molar ratio: 0.75 or FUR/H_2O molar ratio: 3).

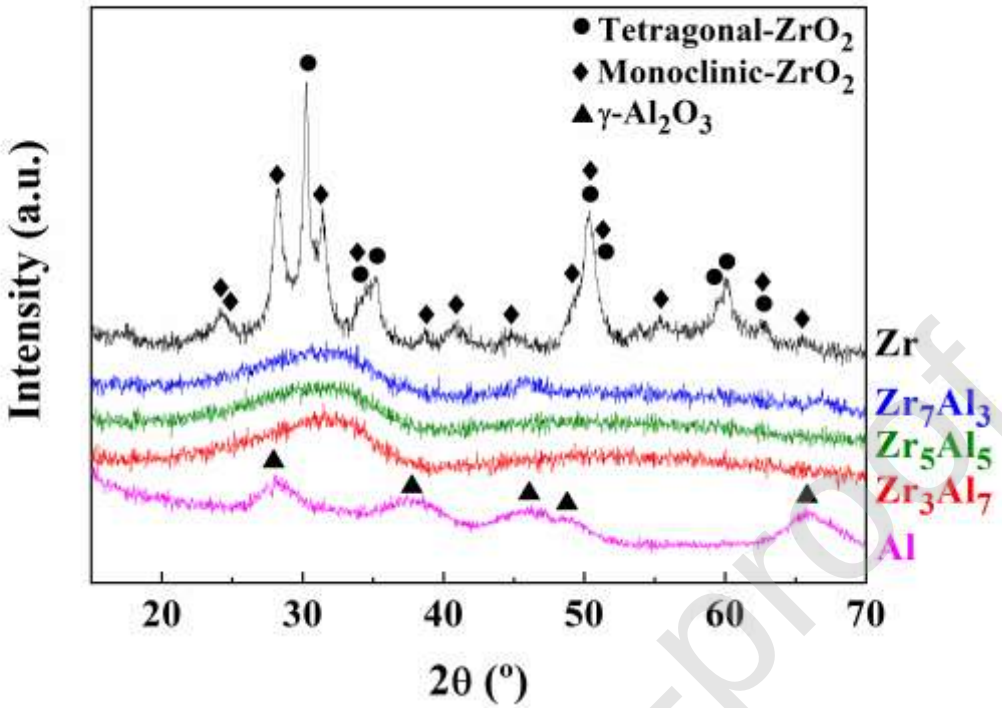

Figure 1

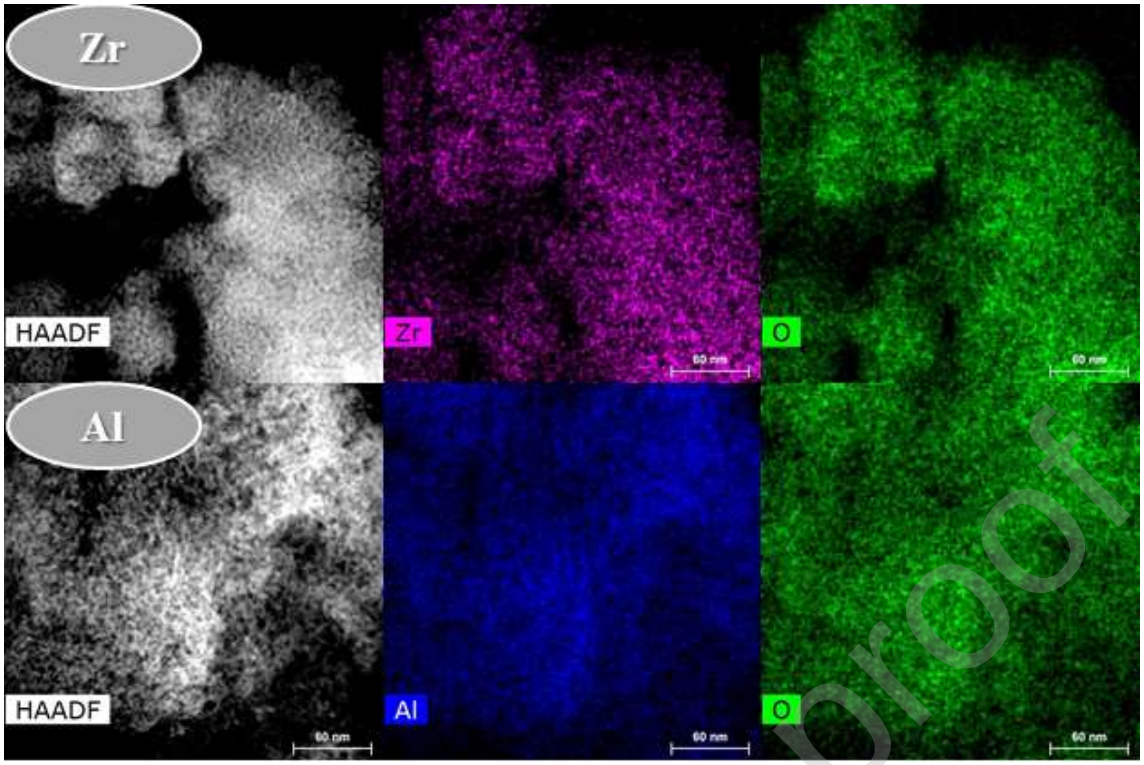

Figure 2

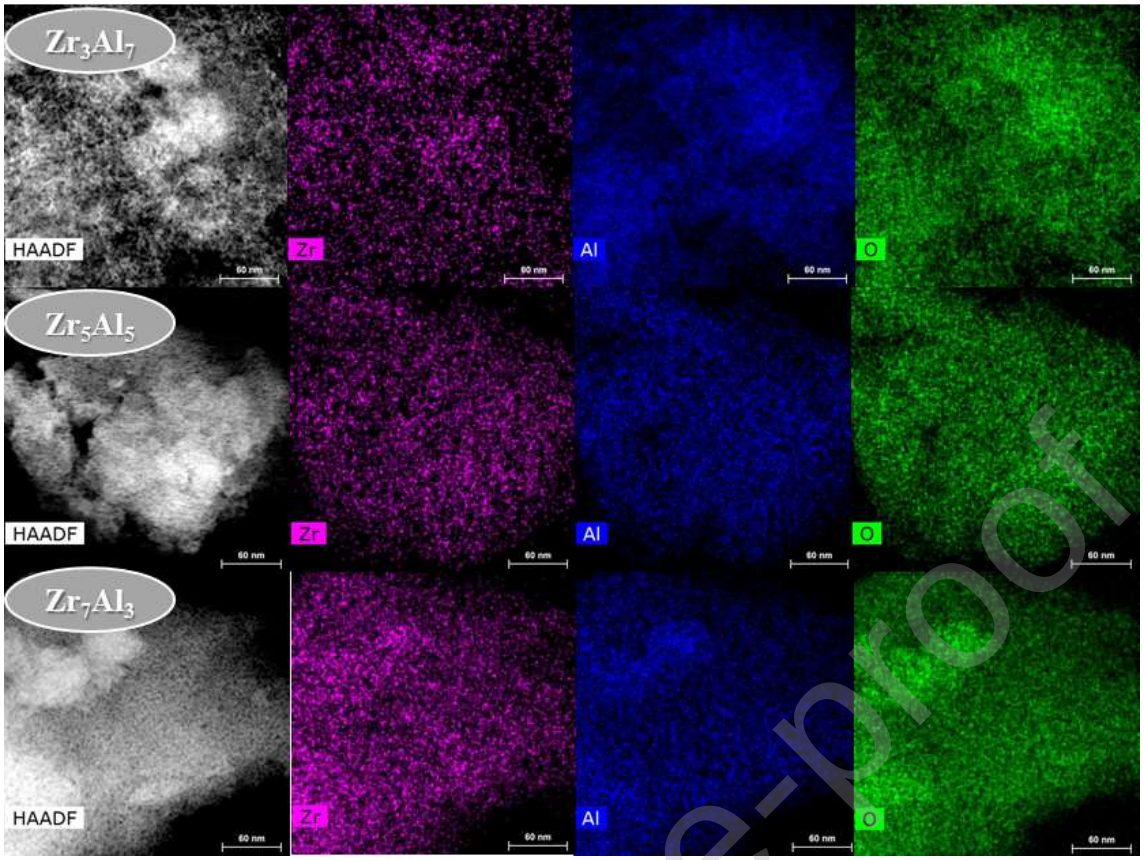

Figure 2. Continuation

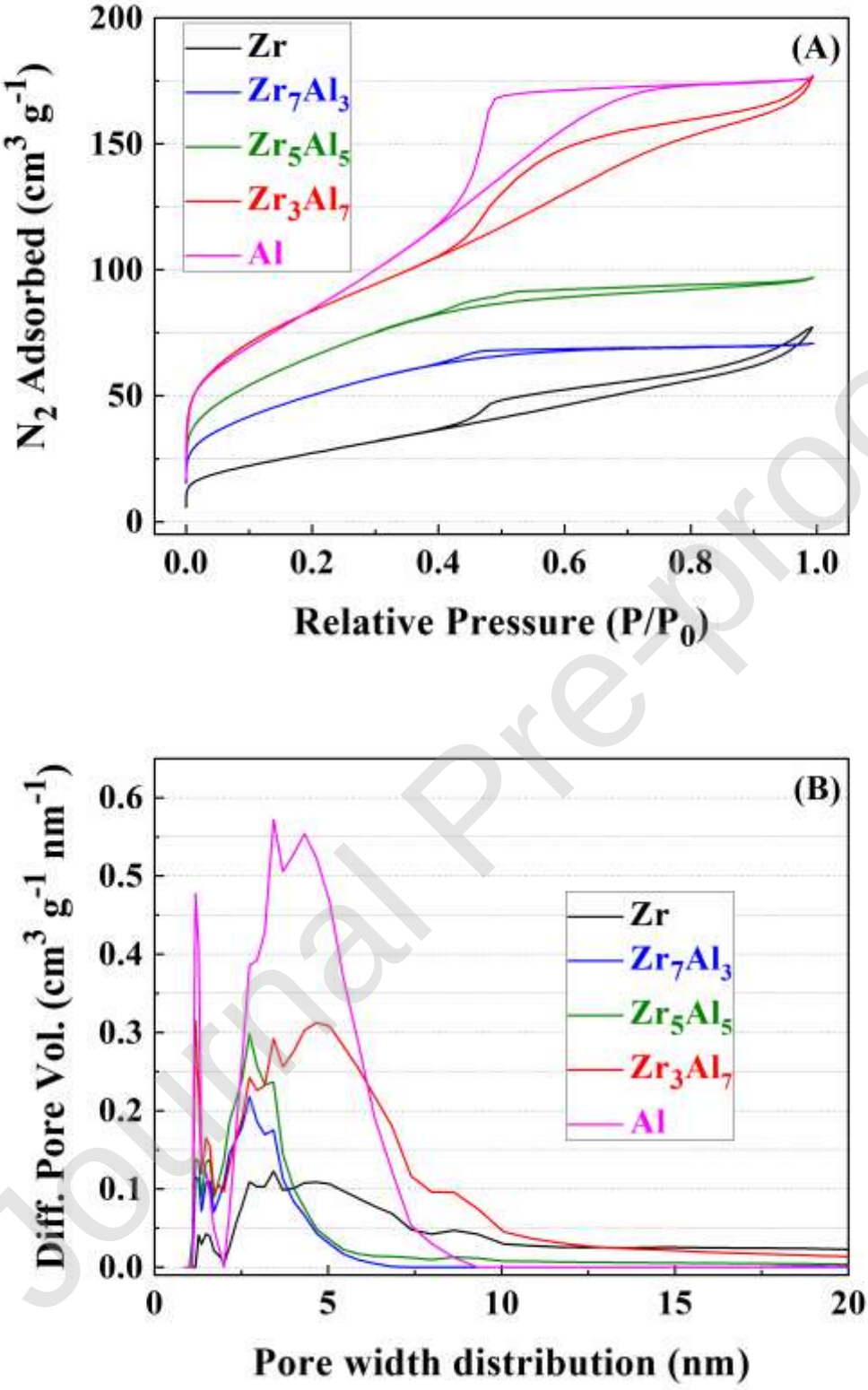

Figure 3

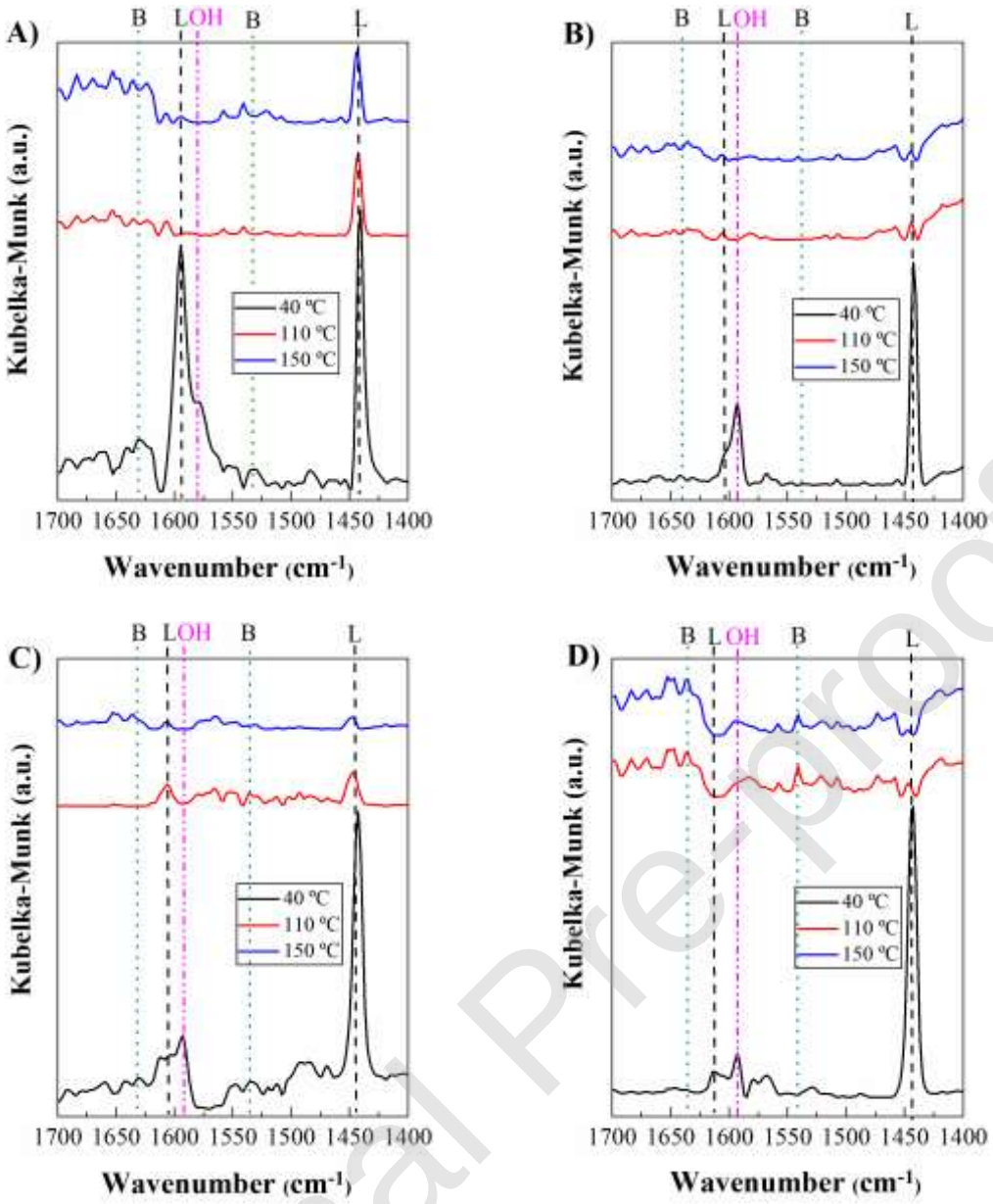

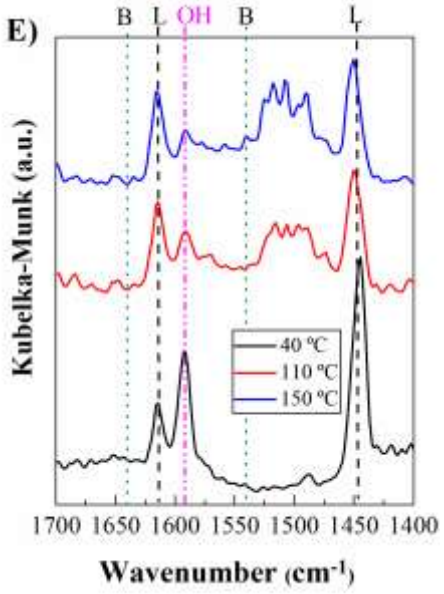

Figure 4

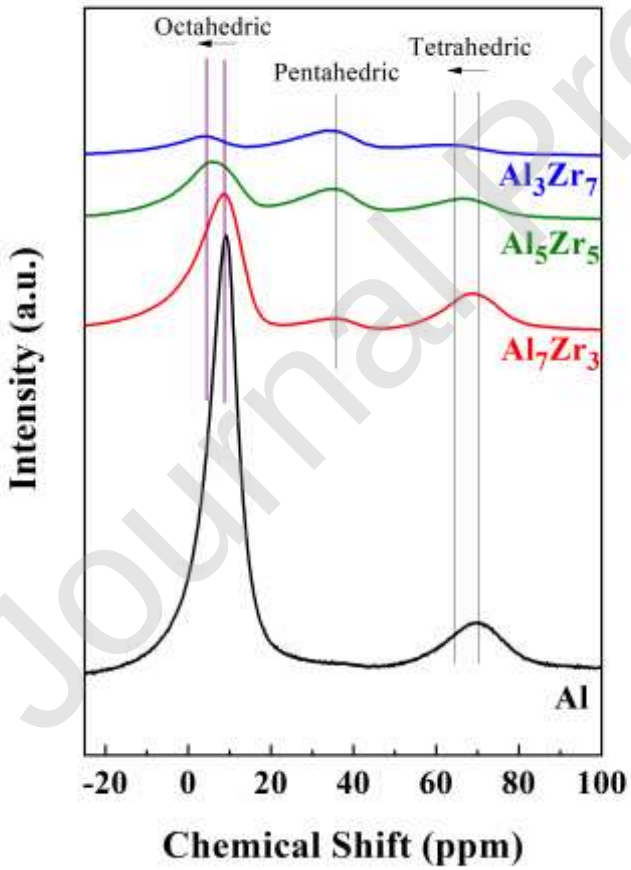

Figure 5

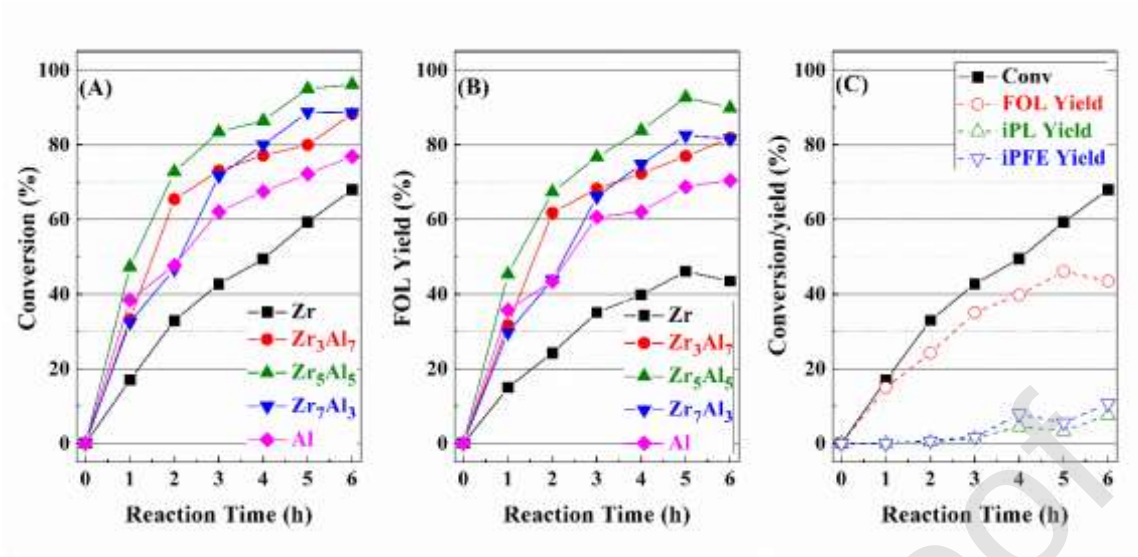

Figure 6

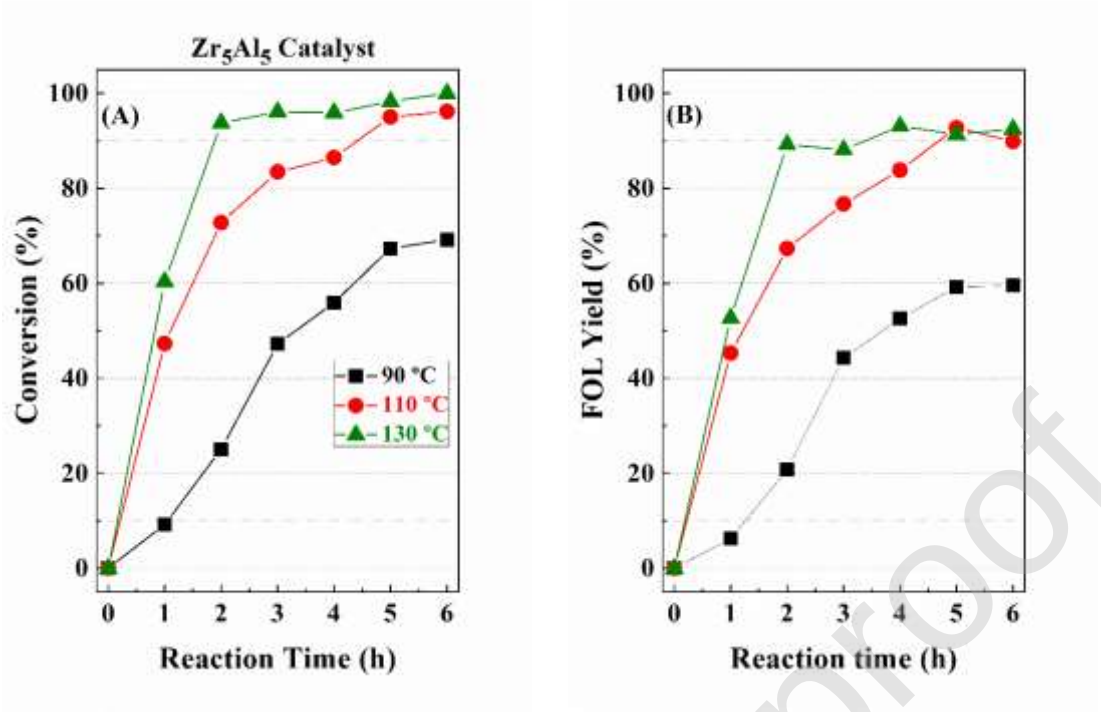

Figure 7

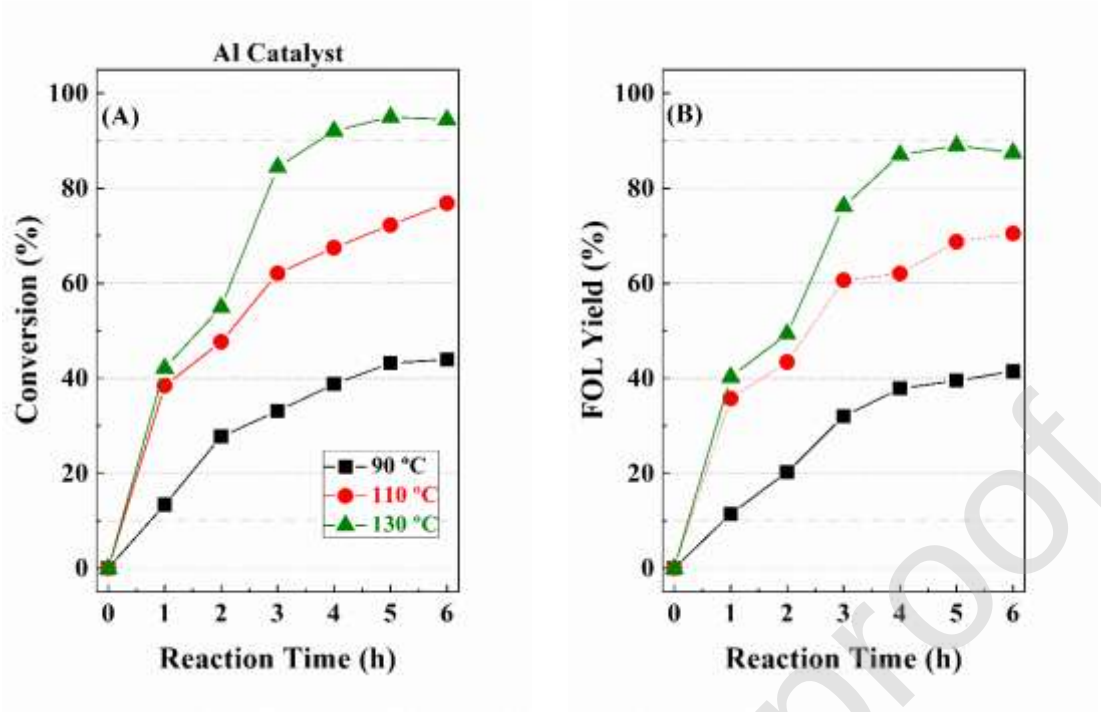

Figure 8

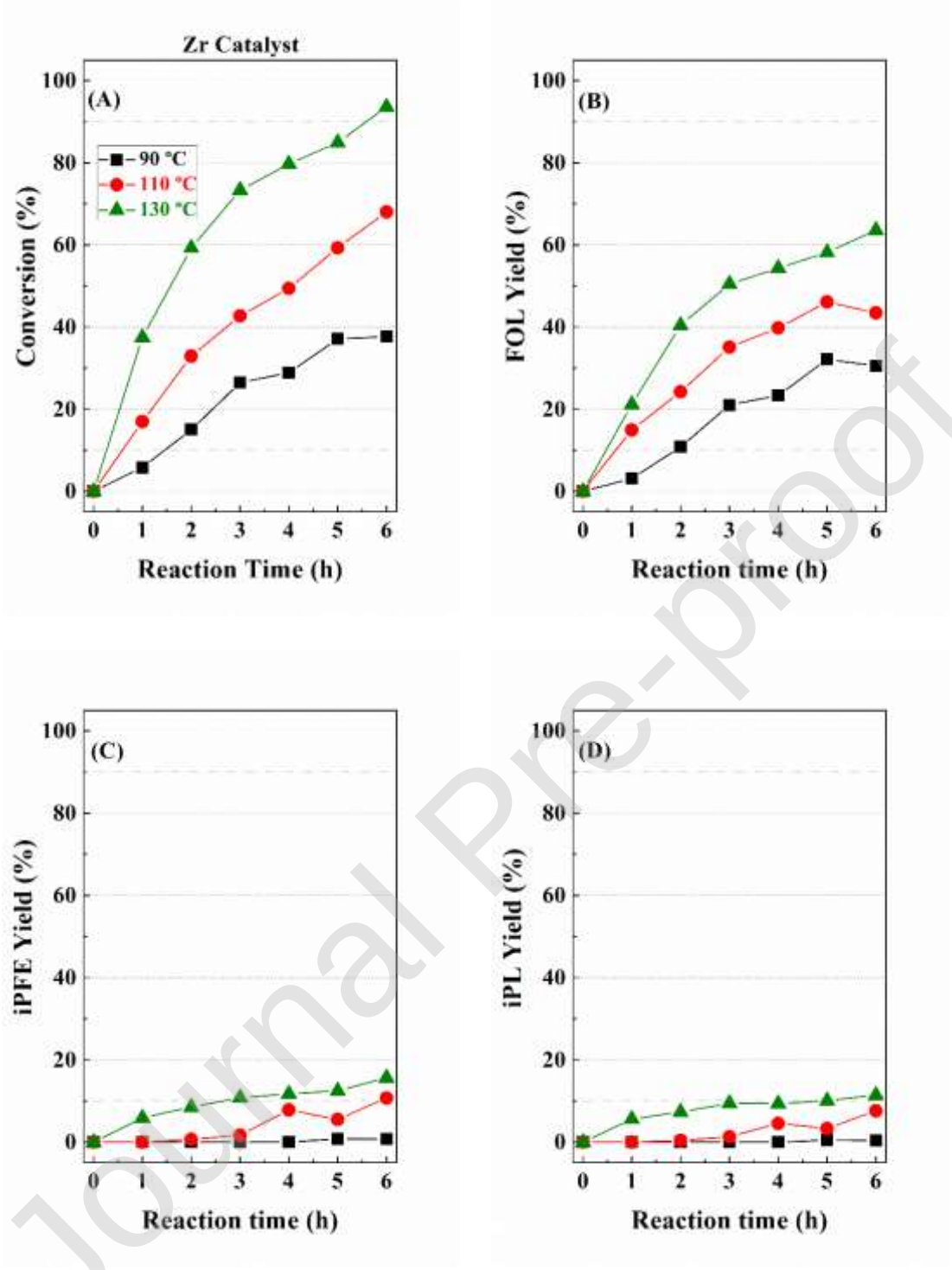

Figure 9

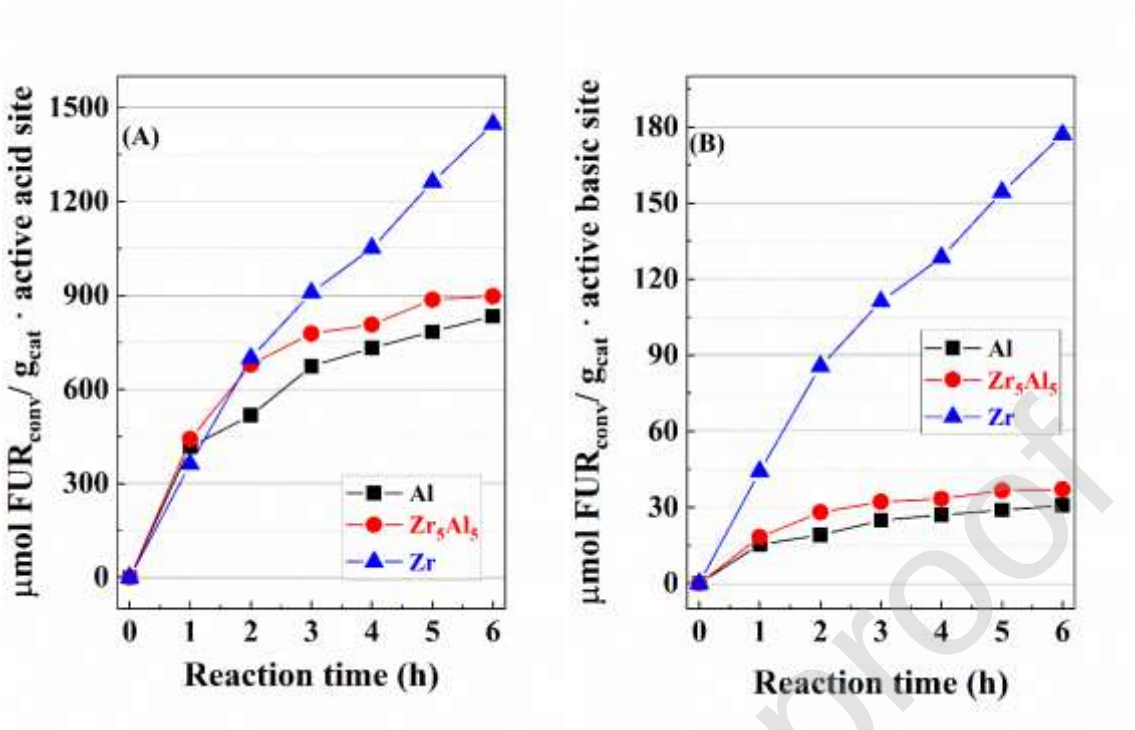

Figure 10

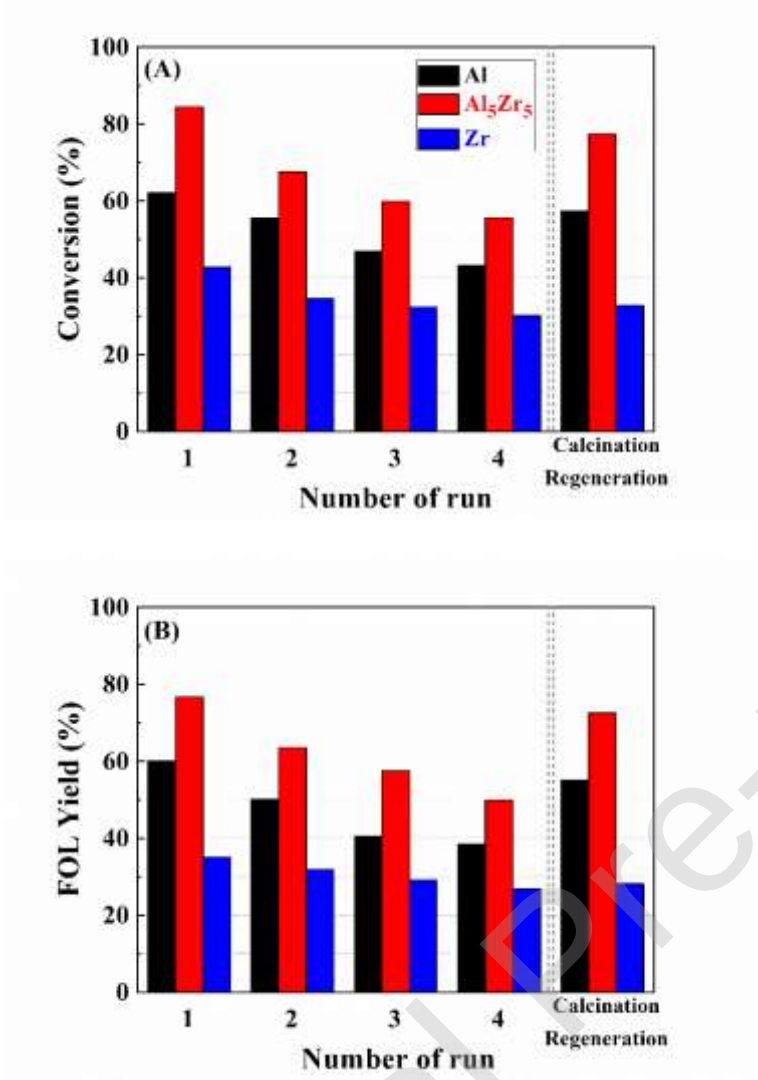

Figure 11

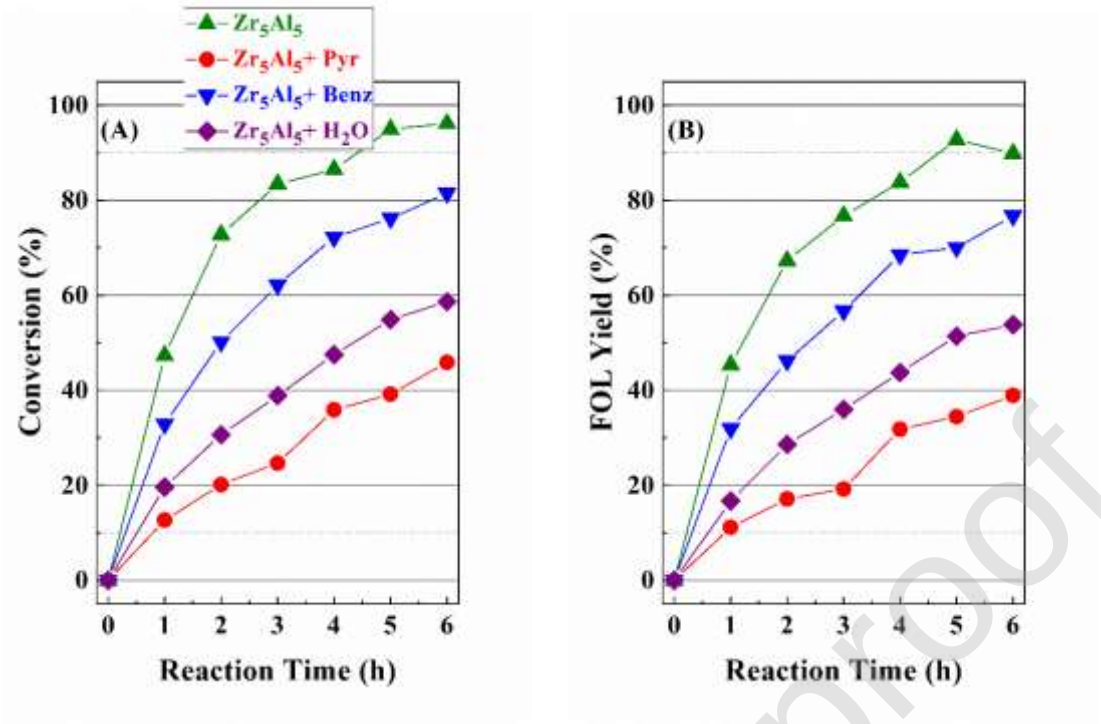

Figure 12

Table 1. Textural properties of Zr, Zr_xAl_y and Al catalysts.

Catalyst	**S_{BET} ($m^2\ g^{-1}$)**	***t*-plot ($m^2\ g^{-1}$)**	**V_P ($cm^3\ g^{-1}$)**	**V_{microp} ($cm^3\ g^{-1}$)**
Zr	101	12	0.10	0.01
Zr_7Al_3	184	127	0.11	0.06
Zr_5Al_5	241	167	0.15	0.08
Zr_3Al_7	304	175	0.26	0.09
Al	312	185	0.27	0.10

Table 2. Acid-base properties for Zr, Zr_xAl_y and Al catalysts.

Catalyst	**NH_3 chemisorbed (µmol g^{-1})**				**CO_2 chemisorbed (µmol g^{-1})**
	Total	Weak (100-200 ºC)	Medium (300-400 ºC)	Strong (> 400 ºC)	Total
Zr	489	221	233	35	4
Zr_7Al_3	780	414	335	31	11
Zr_5Al_5	1115	522	472	120	27
Zr_3Al_7	966	421	425	20	39
Al	959	382	438	139	26

Table 3. Spectral parameters, atomic concentration and superficial molar ratio on the Surface of Zr, Zr_xAl_y and Al catalysts (determined by XPS).

Catalyst	Binding energy (eV) Atomic concentrations (%)				Superficial molar ratio	
	C 1S	O 1s	Al 2p	Zr 3d	Al/Zr ratio	Al/Zr theoretical ratio
Zr	284.8 eV (8.47%)	532.0 eV (62.26%)	-	182.2 eV (29.25%)	-	-
Zr_7Al_3	284.8 eV (8.11%)	531.8 eV (64.42%)	74.6 eV (9.12%)	182.9 eV (25.97%)	0.35	0.43
Zr_5Al_5	284.8 eV (9.70%)	531.5 eV (61.29%)	74.9 eV (14.60%)	182.9 eV (14.39%)	1.01	1.00
Zr_3Al_7	284.8 eV (4.87%)	531.4 eV (61.49%)	74.6 eV (23.73%)	182.7 eV (9.93%)	2.38	2.30
Al	284.8 eV (11.12%)	531.4 eV (62.79%)	74.6 eV (26.08%)	-	-	-